Cornering top-philic dark matter with colliders and cosmology: the importance of QCD corrections

Benjamin Fuks[1,2]

[1] Laboratoire de Physique Théorique et Hautes Energies (LPTHE), UMR 7589, Sorbonne Université et CNRS, 4 place Jussieu, 75252 Paris Cedex 05, France
[2] Institut Universitaire de France, 103 boulevard Saint-Michel, 75005 Paris, France

E-mail: fuks@lpthe.jussieu.fr

Abstract. Constraining dark matter models necessitates accurate predictions for large set of observables originating from collider physics, cosmology and astrophysics. We consider two classes of top-philic dark matter models where the dark sector is coupled to the Standard Model via the top quark and study the complementarity of dark matter relic density, direct and indirect detection and collider searches in exploring the model parameter space. We moreover investigate how higher-order corrections affect the results.

1. Introduction

Dark matter is convincingly evidenced by numerous measurements and observations, like the cosmic microwave background, the flattening of the galaxy rotation curves or gravitational lensing. These many hints triggered a huge endeavour to detect dark matter and study its properties in experiments that range from direct and indirect probes to collider searches. However, despite this huge experimental effort, there is currently no indication about the true nature of dark matter. As a consequence, dark matter scenarios are more and more constrained by many complementary datasets. We illustrate the impact of this complementarity for models in which dark matter is top-philic, *i.e.* when it dominantly couples to top quarks [1, 2]. We moreover assess the impact of QCD higher-order corrections on the predictions, both for collider processes and dark matter annihilation in the universe. In Section 2, we focus on cosmological constraints, whilst Section 3 is dedicated to collider constraints. We conclude by combining these two sets of constraints in Section 4.

2. Probing top-philic dark matter with cosmology

For concreteness, we consider a simplified top-philic dark matter scenario in which the dark matter particle is a scalar S of mass m_S and interacts with the top quark t through a Yukawa interaction $\tilde{y}_t$ involving a vector-like quark T of mass m_T. We moreover impose a $\mathbb{Z}_2$ discrete symmetry under which all Standard Model fields are even and new physics states odd, which guarantees dark matter stability and forbids any mixing of the heavy quark with the top quark. This model is described by the Lagrangian

$$\mathcal{L} = \mathcal{L}_{\rm SM} + i\bar{T}\not{\partial}T - m_T\bar{T}T + \frac{1}{2}\partial_\mu S\partial^\mu S - \frac{1}{2}m_S S^2 + \left[\tilde{y}_t\, S\, \bar{T}P_R t + \text{h.c.}\right], \qquad (1)$$

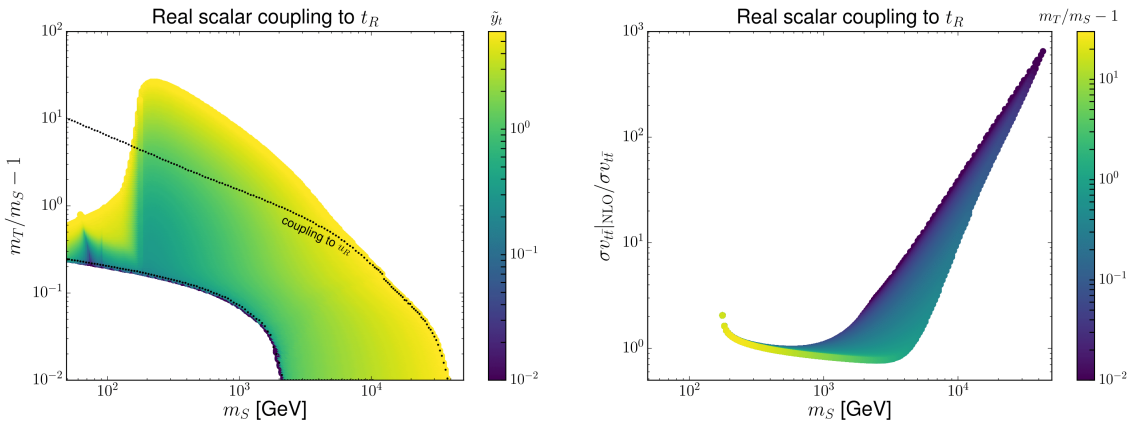

Figure 1. Left: Region of the parameter space in which the measured relic abundance can be accommodated by fixing $\tilde{y}_t$ (given through the colour code). The results are presented in the $(m_S, r-1)$ plane. For comparison, the dotted black contour represents the viable parameter space region obtained when the top mass is neglected. Right: Ratio of the NLO annihilation cross section into top-antitop pairs to the LO one. Figures from Ref. [2].

where P_R denotes the right-handed chirality projector, $\mathcal{L}_{\rm SM}$ the Standard Model Lagrangian, and where any coupling of dark matter to the Higgs sector is considered vanishing. The model parameter space is then defined by three parameters that we choose to be the dark matter mass m_S, the compression factor of the spectrum $r - 1 = m_T/m_S - 1$ and the Yukawa coupling $\tilde{y}_t$.

2.1. Relic abundance

In order to determine the dark matter relic abundance, we assume standard cosmology and a thermal freeze-out mechanism to describe dark matter dynamics in the early universe. The annihilation cross section is evaluated by including all tree-level $2 \to 2$ diagrams, to which we supplement contributions from dark matter annihilations into a three-body tWb system, Sommerfeld enhancement, annihilations into gluons and photons as well as next-to-leading-order (NLO) QCD corrections to the annihilation cross section into top-antitop pairs. Whilst threshold corrections should in principle be included as affecting the production of a top-antitop system at rest [3], they are expected to yield subleading corrections due to the absence of any toponium bound state. They are thus omitted. In the left panel of Figure 1, we present numerical predictions obtained with MicrOMEGAs [4], after having modified the program to accomodate the above-mentioned features. We show the region of the $(m_S, r-1)$ plane for which there exists a value of the Yukawa coupling $\tilde{y}_t$, indicated through the colour code, that yields a relic density $\Omega h^2 = 0.12$ compatible with Planck data [5]. Our results ignore scenarios featuring a $\tilde{y}_t$ coupling smaller than 10^{-4} and larger than 6, the former being associated with a too naive treatment of co-annihilations by MicrOMEGAs [6] and the latter corresponding to a potential breakdown of perturbation theory.

For very heavy dark matter with $m_S > 5$ TeV, dark matter annihilations into top quarks dominate. The top mass m_t however plays a subleading role, the viable region of the parameter space (coloured area) matching the contour obtained when m_t is neglected (dotted black). In this kinematical regime, the annihilation cross section is entirely driven by NLO effects, as illustrated on the right panel of Figure 1 where we present K-factors defined as the ratio of the NLO result to the leading-order (LO) one for all viable scenarios. The huge K-factors representative of the $m_S > 5$ TeV region are driven by virtual internal bremsstrahlung (VIB)

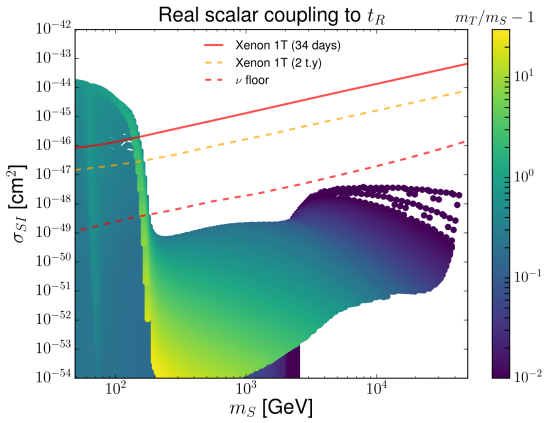

Figure 2. Spin-independent dark matter scattering cross section as a function of the dark matter mass m_S. For each scenario, the $\tilde{y}_t$ value is set to reproduce the observed relic density and the compressibility factor is depicted by the colour code. We indicate current (solid red) and future (dashed orange) 90% confidence level exclusions by the Xenon 1T experiment [10,11]. The dashed red line corresponds to the neutrino floor. Figure from Ref. [2].

diagrams [7–9]. Final-state radiation is indeed helicity suppressed (as proportional to m_t/m_S), in contrast to VIB emission that is proportional to m_T/m_S and thus enhanced as the spectrum is compressed in this parameter space region (see the colour code in the figure). For moderate dark matter masses $m_t < m_S < 5$ TeV, annihilations into top quarks still dominate but the behaviour is this time driven by tree-level S-wave contributions, the NLO corrections being small (K-factors of $\mathcal{O}(1)$). In the massless limit, annihilations into quark pairs are negligible and the relic density is driven by loop-induced annihilations into gluons (dotted black contour in the left panel of Figure 1). In contrast, in the massive case, significant annihilations into quarks allow for larger $r-1$ choices to accommodate the measured relic density (coloured contour). In the light dark matter case ($m_S < m_t$), the relic density is governed by annihilations into a tWb system or gluons, or through co-annihilations with the mediator for more compressed scenarios. Co-annihilations play an important role near $m_T + m_S \simeq m_t$ as they are resonantly enhanced, which corresponds to the dark blue region in the left panel of Figure 1 ($m_S \sim 70 - 80$ GeV). Annihilations into gluons are only relevant when all co-annihilation channels are closed (*i.e.* for very light dark matter), and annihilations into a tWb system only contribute close to threshold for $m_S \in [(m_t + m_W)/2, m_t]$.

2.2. Direct detection

In the scenario studied in this section, dark matter scattering off nuclei proceeds via loop-induced interactions with the gluon field strength tensor $G_{\mu\nu}$, that could be modelled effectively [12],

$$\mathcal{L}_g = \frac{\tilde{y}_t^2}{48\left[m_T^2 - m_S^2\right]} \frac{\alpha_s}{\pi} S^2 G_a^{\mu\nu} G_{\mu\nu}^a \,. \tag{2}$$

Accounting for a nucleus of mass m_A and comprised of Z protons p and $(A-Z)$ neutrons n, the spin-independent dark matter scattering cross section $\sigma_{\rm SI}$ is derived from the coherent sum of the proton and the neutron contributions,

$$\sigma_{\rm SI} = \frac{m_A^2}{\pi(m_S + m_A)^2} \Big[Z f_p + (A-Z) f_n \Big]^2 \quad \text{with} \quad \frac{f_N}{m_N} = -\frac{\tilde{y}_t^2}{54\left[m_T^2 - m_S^2\right]} \Big[1 - \sum_{q=u,d,s} f_{T_q}^{(N)} \Big] \,. \tag{3}$$

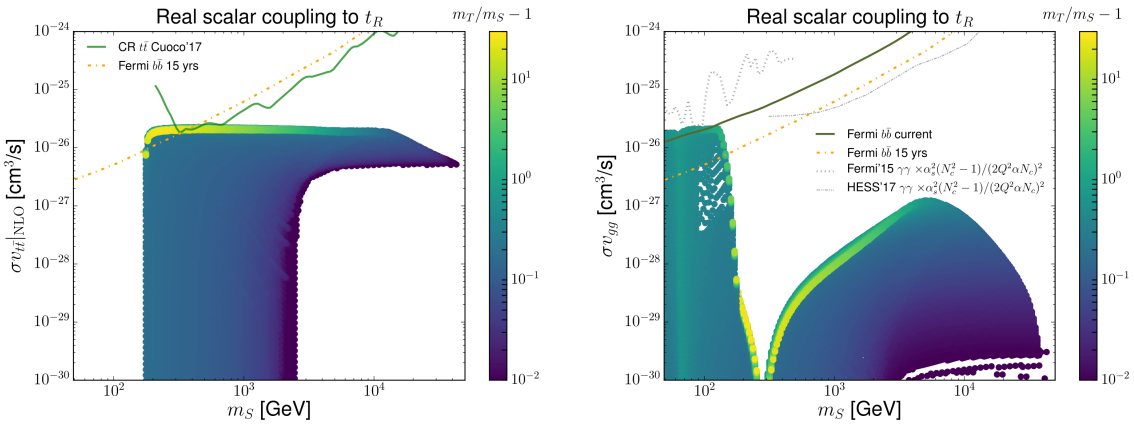

Figure 3. NLO $SS \to t\bar{t}$ (left) and loop-induced LO $SS \to gg$ (right) annihilation cross sections at zero velocity. We indicate the limits obtained from cosmic rays (solid light green), and from the analysis of current (solid dark green) and future (dot-dashed orange) Fermi-LAT dwarf spheroidal galaxy data in the $b\bar{b}$ channel. Upper limits obtained from the gamma-ray analysis of H.E.S.S. (double-dotted dashed grey) and Fermi-LAT (dotted grey) are also shown. For each scenario, the $\tilde{y}_t$ value is set to reproduce the observed relic density and the compressibility factor is depicted by the colour code. Figures from Ref. [2].

This expression depends on the coupling f_N of S to a nucleon N of mass m_N, that is related to the quark mass fractions $f_{T_q}^{(N)}$ deduced from lattice calculations [13].

In Figure 2, we present the m_S-dependence of $\sigma_{\rm SI}$ for all viable scenarios featuring a relic density in agreement with Planck data. Below the top threshold, the largest cross section values are obtained for setups in which the relic density is driven by annihilations into gluons and for which $\tilde{y}_t$ is large. Above the top threshold, the $\tilde{y}_t$ value necessary to get the right relic abundance drops, and so does $\sigma_{\rm SI}$. On different lines, $St \to Tg$ co-annihilations impact the results for $m_S \gtrsim 2.5$ TeV, yielding an enhancement of the scalar interactions with gluons in $\mathcal{L}_g$. For most scenarios, $\sigma_{\rm SI}$ lies below the neutrino floor and is thus not reachable by direct detection experiments. For spectrum featuring light dark matter annihilating into gluons, many scenarios are however within the present (34 days of exposure) and future (2.1 years of data acquisition) reach of Xenon 1T [10, 11].

2.3. Indirect detection

In Figure 3 we present, for all viable scenarios, predictions for the dark matter annihilation cross section at zero velocity for a top-antitop ($\sigma v_{t\bar{t}}$, left panel) and gluon-pair (σv_{gg}, right panel) final state. The respective cross sections are evaluated at the NLO and loop-induced LO accuracy in QCD. As already found in the previous subsections, annihilations into gluons are only relevant below the top threshold, and annihilations into top-antitop pairs dominate for $m_S > m_t$. We moreover recall that NLO effects largely affect the predictions for $m_S > 5$ TeV (see Section 2.1).

Dark matter annihilations into top-antitop pairs can be constrained from antiproton cosmic ray fluxes [14] (solid light green line), and annihilations into both top quarks and gluons can be constrained by the analysis of gamma-ray Fermi-LAT dwarf spheroidal data in the $b\bar{b}$ mode [15] (solid dark green line). Similarly, the future gamma-ray sensitivity to the model can be extrapolated after accounting for the prospects of 15 years of Fermi-LAT running [16] (dot-dashed orange lines). Although there is no direct Fermi-LAT results for annihilations into the considered final states, the subsequent secondary gamma-ray spectrum is expected to exhibit a

similar behaviour as for annihilations into a $b\bar{b}$ system [2]. An estimate of the limits can therefore be extracted through a reweighting procedure [17],

$$\sigma v_{gg,t\bar{t}} = \sigma v_{b\bar{b}} \frac{N_\gamma^{b\bar{b}}}{N_\gamma^{gg,t\bar{t}}} \ , \tag{4}$$

where N_γ^X is the number of photons originating from an X final state that we estimate from the hadronisation model implemented in the Pythia 8 package [18].

H.E.S.S. [19] (double-dot-dashed grey line) and Fermi-LAT gamma-ray data [20] (dashed grey line) can potentially constrain the model when considering direct dark matter annihilations into photons. The latter is expected to be enhanced in two regimes, *i.e.* for light dark matter ($m_S < m_t$) where loop-induced annihilations into photons could be important (most other channels being closed) and in the multi-TeV regime where radiative emission is dominated by VIB diagrams. The corresponding cross sections, associated with dark matter annihilations into photons and into a $t\bar{t}\gamma$ system, can be deduced from

$$\sigma v_{\gamma\gamma} = \frac{4Q^4\alpha^2 N_c^2}{\alpha_S^2\,(N_c^2-1)} \sigma v_{gg} \qquad \text{and} \qquad \sigma v_{t\bar{t}\gamma} = \frac{2N_c Q^2 \alpha}{(N_c^2-1)\alpha_s} \sigma v_{t\bar{t}g} \ , \tag{5}$$

where $N_c = 3$ denotes the number of colours, α and α_S the electromagnetic and strong coupling, and Q the electric charge of the heavy quark T. The predictions can be confronted to the results of Fermi-LAT at energies around and below m_t as well as to the results of H.E.S.S. for larger dark matter masses (following the procedure of Ref. [21]).

As shown in Figure 3, present and future gamma-ray and cosmic-ray data turns out to be sensitive to only a small fraction of the model parameter space.

3. Collider constraints on top-philic dark matter

In full generality, top-philic dark matter models can be probed at colliders via several processes [1]. First, dark matter can be produced from (virtual or resonant) mediator exchanges, potentially together with one or more Standard Model particles. Whilst dark matter is stable and leaves a missing energy signature in the detector, the extra Standard Model objects are visible and provide handles on new physics. Next, depending on the details of the model, mediator production can also resonantly leads to a purely Standard Model final state, which offers hence another set of probes of the model.

The dark matter model detailed in Section 2 does not give rise to the most general phenomenology as it cannot be probed through resonance searches in Standard Model final states. We therefore focus on a different model that can be probed through both dark matter searches and resonance searches. We illustrate this feature, as well as the impact of the QCD corrections, by studying, for the sake of the example, LHC Run 1 results. The final results on the model of the previous section will nevertheless include LHC Run 2 data and will be shown in Section 4. We consider a simplified top-philic dark matter model built by supplementing the Standard Model with a Dirac fermionic dark matter field χ of mass m_X and a scalar mediator Y_0 of mass m_Y. The interactions are described by the Lagrangian

$$\mathcal{L} = \mathcal{L}_{\rm SM} + \mathcal{L}_{\rm kin} - \Big(g_t \frac{y_t}{\sqrt{2}} \bar{t}t + g_X \bar{\chi}\chi \Big) Y_0 \ , \tag{6}$$

in which we denote by g_t and g_X the coupling strengths of the mediator to the Standard Model and dark sector respectively. We have assumed that the mediator couples to fermions with a strength proportional to the corresponding Yukawa coupling y_f, so that only the top quark can be considered, and $\mathcal{L}_{\rm kin}$ includes new physics kinetic and mass terms.

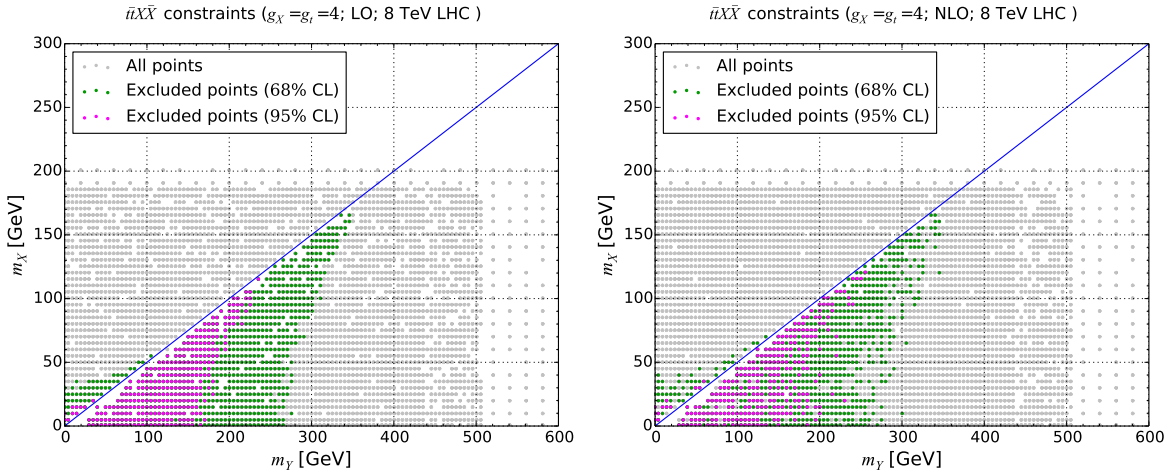

Figure 4. LHC Run 1 sensitivity to the considered model (with $g_t = g_X = 4$) based on the CMS dark matter analysis in the top-antitop plus missing energy channels. Signal simulations are achieved at LO (left) and NLO (right) in QCD. Figures from Ref. [1].

For our collider simulations, we have implemented the above Lagrangian into FeynRules [22], which we have jointly used with NLOCT [23] to generate an NLO UFO model [24]. We have made use of MG5_aMC@NLO [25] to generate hard-scattering events obtained by the convolution of LO and NLO matrix elements with the NNPDF 2.3 set of parton distribution functions [26]. The resulting events are matched with parton showers as modeled by Pythia 8 [18], that is also used to describe hadronisation. The response of the LHC detectors is handled by Delphes 3 [27] that is tuned appropriately [28], and signal efficiencies and exclusion contours are estimated by reinterpreting the results of various LHC analyses with MadAnalysis 5 [29–31].

3.1. Searches with missing transverse energy

Top-philic dark matter can be explored at colliders through a signature comprised of a top-quark pair and missing energy. We focus on the corresponding Run 1 CMS analysis [32]. In order to examine the impact of the QCD corrections on the sensitivity, we first fix the new physics couplings $g_t = g_X = 4$ and scan over the mediator and dark matter masses m_Y and m_X. The results are shown in Figure 4 when LO (left panel) and NLO (right panel) signal simulations are considered, and mass configurations excluded at the 68% (green) and 95% (magenta) confidence level (CL) are indicated. All excluded points (at the 95% CL) lie in the triangular low-mass region where the mediator is heavy enough to resonantly decays into a pair of dark matter particles, which corresponds to the region with the largest signal cross section. Scenarios featuring mediator masses ranging up to about 200–250 GeV are excluded, especially if the mediator decays close to threshold ($m_Y \sim 2m_X$). Further from threshold, the mediator width can become large by virtue of the large coupling choice, so that the excluded region is not exactly triangular and the signal fiducial cross section acquires a dark matter mass dependence.

As NLO corrections have a mild effect on the shape of the relevant signal distributions [33], their impact is entirely driven by changes in the signal rates. We observe that in the low-mass region (where the K-factor is found to be of about 1.10), the exclusion contours do not feature any significant effect. For larger m_Y values, the K-factors are of about 1 and the exclusion region is identical at LO and NLO. NLO corrections are however expected to significantly reduce theoretical uncertainties. In order to study this, we select the three benchmark scenarios

Table 1. Benchmark scenarios used to determine the NLO impact on the sensitivity of the Run 1 CMS search for dark matter in the top-antitop plus missing energy channel. LO and NLO cross sections are shown together with the CLs exclusions, all results including scale uncertainties.

	$(m_Y,\, m_X)$	$\sigma_{\rm LO}$ [pb]	$\mathrm{CL}_{\rm LO}$ [%]	$\sigma_{\rm NLO}$ [pb]	$\mathrm{CL}_{\rm NLO}$ [%]
I	(150, 25) GeV	$0.658^{+34.9\%}_{-24.0\%}$	$98.7^{+0.8\%}_{-13.0\%}$	$0.773^{+6.1\%}_{-10.1\%}$	$95.0^{+2.7\%}_{-0.4\%}$
II	(40, 30) GeV	$0.776^{+34.2\%}_{-24.1\%}$	$74.7^{+19.7\%}_{-17.7\%}$	$0.926^{+5.7\%}_{-10.4\%}$	$84.2^{+0.4\%}_{-14.4\%}$
III	(240, 100) GeV	$0.187^{+37.1\%}_{-24.4\%}$	$91.6^{+6.4\%}_{-18.1\%}$	$0.216^{+6.7\%}_{-11.4\%}$	$86.5^{+8.6\%}_{-5.5\%}$

presented in Table 1 together with the corresponding LO and NLO signal cross sections and the CLs exclusions. We additionally indicate the scale uncertainty bands that have been obtained by varying the central scale, set to the average transverse mass of all final state particles, by a factor of 2 up and down. Using NLO predictions leads to a significant reduction of the uncertainties in the total cross section, compared with the LO case, which propagates down to the CLs exclusions. NLO predictions therefore allow us to draw more reliable conclusions on the viability of a parameter space point.

Mono-X signals, in which a pair of dark matter particles is produced together with a Standard Model particle X, can also be relevant for obtaining bounds on dark matter models. Amongst all these searches, we consider the monojet one given the relative magnitude of the strong and electroweak couplings. As an example, we use the Run 1 CMS monojet analysis [34] and signal simulations at LO (as loop-induced). In our recasting procedure, we conservatively select the signal region driving the strongest bound. The results are shown in the left panel of Figure 5 for $g_t = g_X = 4$, in which we represent scenarios excluded at the 68% (green) and 95% (magenta) CL. Most excluded scenarios lie again in the triangular low-mass region of the parameter space, in which the mediator resonantly decays into a pair of dark matter particles. Except for the small subset of points excluded at the 68% CL for setups where $m_Y < 2m_X$, the boundaries of the excluded region are derived from the significant reduction of the monojet fiducial cross section that rapidly falls with m_Y once the top threshold is crossed. The LHC Run 1 is therefore not sensitive to mediator heavier than 500 GeV. In the offshell $m_Y < 2m_X$ regime, jets are harder [35], so that the signal selection efficiency is larger and such scenarios can be reached. The monojet search is overall found to be more constraining than the top-antitop plus missing energy one, especially for heavier mediator thanks to the larger monojet cross section.

3.2. Searches without missing transverse energy

Dark matter models can also be constrained by resonance searches when the new physics resonance decays into a pair of Standard Model particles, as mediators can sometimes decay back into the Standard Model sector. Dijet and diphoton resonance searches could in principle constrain the considered model. However, due to the double-loop suppression stemming from the mediator couplings to gluons and photons, new physics contributions to dijet and diphoton production are only relevant for $m_Y < 2\,\min(m_X, m_t)$, *i.e.* when the mediator cannot decay into top quarks and dark matter. Due to the large QCD background and trigger reasons, LHC dijet resonance searches target high invariant-mass dijet systems, so that the lowest mediator mass that could be reached by Run 1 data is of about 500 GeV, the corresponding cross section bound being 10 pb [36]. This consequently yields no constraint on the model. In contrast, despite the small mediator branching ratio into a diphoton final state, diphoton probes can potentially constrain the model due to the low level of associated backgrounds. In the right panel of Figure 5, we present, in the (m_Y, g_t) plane, the constraints derived from the results of

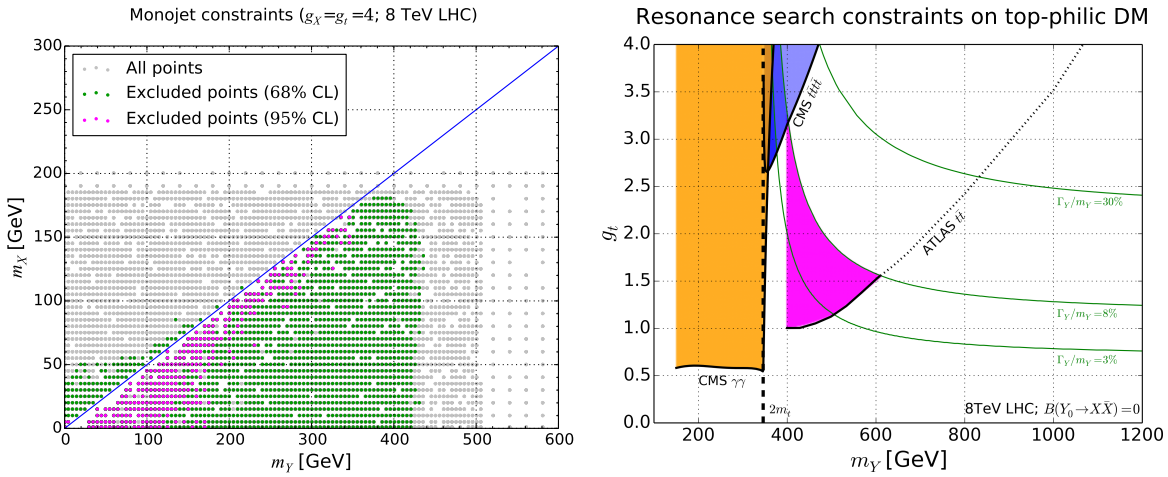

Figure 5. Left: LHC Run 1 monojet constraints on the considered top-philic dark matter model as obtained by reinterpreting the Run 1 CMS monojet search. Right: LHC Run 1 constraints issued from the reinterpretation of new physics searches in the diphoton (orange), $t\bar{t}$ (magenta) and $t\bar{t}t\bar{t}$ (blue) modes. Information on the mediator width to mass ratio is represented by green curves. Figures from Ref. [1].

the Run 1 CMS diphoton search [37] that investigates resonance masses ranging from 150 to 850 GeV. The bounds are obtained by comparing the experimental limits with predictions for single mediator production at the next-to-next-to-leading-order (NNLO) [38].

For scenarios with mediator masses above the top threshold, one relies instead on signatures featuring a $t\bar{t}$ resonance. In our setup, loop-induced single mediator production can enhance top-antitop production, in particular when there is a large coupling hierarchy ($g_t \gg g_X$) or mass hierarchy ($2m_t < m_Y < 2m_X$). We extract constraints from the results of the Run 1 ATLAS $t\bar{t}$ resonance search [39] that restricts the new physics contributions to the $t\bar{t}$ cross section as a function of the mediator mass. Comparing with NNLO signal cross section predictions, we show the obtained constraints in the right panel of Figure 5 (magenta) in the (m_Y, g_t) plane, dark matter being again decoupled. Mediators with masses lying in the [400,600] GeV range are found to be reachable for $g_t \in [1, 4]$. The exact form of the excluded region depends on m_Y and on the validity of the narrow-width approximation that must be enforced to recast the ATLAS limits (green curves). In addition, mediators can also be produced in association with a top-antitop pair, which yields a four-top signal after decay. Large new physics four-top contributions are forbidden [40], and recasting the limits extracted from the CMS analysis of Ref. [41] leads to the weak blue excluded region in Figure 5, as resulting from the steeply decreasing (NLO) signal cross section with m_Y.

4. Summary - the collider-cosmology complementarity

We now go back to the model of Section 2 and jointly apply all the constraints discussed in this paper. Our findings, reported in Figure 6, reflect the nice complementarity of cosmological and collider (LEP as well as LHC Run 1 and 2) constraints on the considered dark matter model. We compare the impact of experimental searches from varied origins by confronting their results to predictions including NLO QCD corrections, the latter being crucial for a good theoretical control. The red region is excluded by dark matter direct detection searches from the Xenon 1T [10] experiment, and the region inside the red dashed line is in principle testable by future direct detection searches as above the neutrino floor. The dark and light green regions are

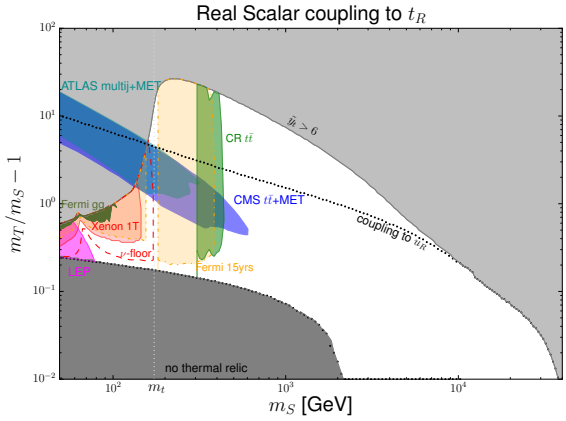

Figure 6. Phenomenologically-viable region of the top-philic dark matter model of Section 2, presented in the $(m_S, r-1)$ plane. The viable region of the parameter space (non-grey regions) is obtained by fixing the $\tilde{y}_t$ coupling to reproduce the observed relic density. We include constraints from direct and indirect dark matter detection as well as from colliders. Figure from Ref. [2].

excluded by Fermi-LAT gamma-ray and cosmic-ray constraints on low and large dark matter masses respectively [14, 15], while the orange area will be testable after 15 years of Fermi-LAT running [16]. Finally, collider searches in the top-antitop plus missing energy channel at LEP [42] and at the LHC [43, 44] are presented as the magenta and light blue contours respectively, and mono-X bounds [45, 46] are given in dark blue.

Our analysis reveals that despite the complementarity between the different sets of constraints, only a small fraction of the parameter space is currently tested. The prospects of all cosmological probes however demonstrate that the most fruitful strategy to further test the model on the longer run would be to increase the energy reach at colliders.

Acknowledgments

I am thankful to the organisers of the Kruger 2018 conference for the invitation and for putting such an inspiring meeting in place. I also warmly thank Alan Cornell for his hospitality at U. Witwatersrand. This study has been partly supported by French state funds managed by the Agence Nationale de la Recherche (ANR) in the context of the LABEX ILP (ANR-11-IDEX-0004-02, ANR-10-LABX-63).

References

[1] Arina C *et al.* 2016 *JHEP* **11** 111 (*Preprint* 1605.09242)
[2] Colucci S, Fuks B, Giacchino F, Lopez Honorez L, Tytgat M H G and Vandecasteele J 2018 *Phys. Rev.* **D98** 035002 (*Preprint* 1804.05068)
[3] Drees M and Hikasa K i 1990 *Phys. Lett.* **B240** 455 [Erratum: Phys. Lett.B262,497(1991)]
[4] Bélanger G, Boudjema F, Pukhov A and Semenov A 2015 *Comput. Phys. Commun.* **192** 322–329 (*Preprint* 1407.6129)
[5] Ade P A R *et al.* (Planck) 2014 *Astron. Astrophys.* **571** A16 (*Preprint* 1303.5076)
[6] Garny M, Heisig J, Lülf B and Vogl S 2017 *Phys. Rev.* **D96** 103521 (*Preprint* 1705.09292)
[7] Giacchino F, Lopez-Honorez L and Tytgat M H G 2013 *JCAP* **1310** 025 (*Preprint* 1307.6480)
[8] Toma T 2013 *Phys. Rev. Lett.* **111** 091301 (*Preprint* 1307.6181)
[9] Colucci S, Giacchino F, Tytgat M H G and Vandecasteele J 2018 *Phys. Rev.* **D98** 115029 (*Preprint* 1805.10173)
[10] Aprile E *et al.* (XENON) 2017 *Phys. Rev. Lett.* **119** 181301 (*Preprint* 1705.06655)
[11] Aprile E *et al.* (XENON) 2016 *JCAP* **1604** 027 (*Preprint* 1512.07501)
[12] Hisano J, Nagai R and Nagata N 2015 *JHEP* **05** 037 (*Preprint* 1502.02244)

[13] Ohki H, Takeda K, Aoki S, Hashimoto S, Kaneko T, Matsufuru H, Noaki J and Onogi T (JLQCD) 2013 *Phys. Rev.* **D87** 034509 (*Preprint* 1208.4185)
[14] Cuoco A, Heisig J, Korsmeier M and Krämer M 2017 (*Preprint* 1711.05274)
[15] Ackermann M *et al.* (Fermi-LAT) 2015 *Phys. Rev. Lett.* **115** 231301 (*Preprint* 1503.02641)
[16] Charles E *et al.* (Fermi-LAT) 2016 *Phys. Rept.* **636** 1–46 (*Preprint* 1605.02016)
[17] Bringmann T, Huang X, Ibarra A, Vogl S and Weniger C 2012 *JCAP* **1207** 054 (*Preprint* 1203.1312)
[18] Sjöstrand T, Ask S, Christiansen J R, Corke R, Desai N, Ilten P, Mrenna S, Prestel S, Rasmussen C O and Skands P Z 2015 *Comput. Phys. Commun.* **191** 159–177 (*Preprint* 1410.3012)
[19] Rinchiuso L, Moulin E, Viana A, Van Eldik C and Veh J (H.E.S.S.) 2017 *PoS* **ICRC2017** 893 (*Preprint* 1708.08358)
[20] Ackermann M *et al.* (Fermi-LAT) 2015 *Phys. Rev.* **D91** 122002 (*Preprint* 1506.00013)
[21] Ibarra A, Lee H M, Lopez Gehler S, Park W I and Pato M 2013 *JCAP* **1305** 016 [Erratum: JCAP1603,no.03,E01(2016)] (*Preprint* 1303.6632)
[22] Alloul A, Christensen N D, Degrande C, Duhr C and Fuks B 2014 *Comput. Phys. Commun.* **185** 2250–2300 (*Preprint* 1310.1921)
[23] Degrande C 2015 *Comput. Phys. Commun.* **197** 239–262 (*Preprint* 1406.3030)
[24] Degrande C, Duhr C, Fuks B, Grellscheid D, Mattelaer O and Reiter T 2012 *Comput. Phys. Commun.* **183** 1201–1214 (*Preprint* 1108.2040)
[25] Alwall J, Frederix R, Frixione S, Hirschi V, Maltoni F, Mattelaer O, Shao H S, Stelzer T, Torrielli P and Zaro M 2014 *JHEP* **07** 079 (*Preprint* 1405.0301)
[26] Ball R D *et al.* 2013 *Nucl. Phys.* **B867** 244–289 (*Preprint* 1207.1303)
[27] de Favereau J, Delaere C, Demin P, Giammanco A, Lemaître V, Mertens A and Selvaggi M (DELPHES 3) 2014 *JHEP* **02** 057 (*Preprint* 1307.6346)
[28] Dumont B, Fuks B, Kraml S, Bein S, Chalons G, Conte E, Kulkarni S, Sengupta D and Wymant C 2015 *Eur. Phys. J.* **C75** 56 (*Preprint* 1407.3278)
[29] Conte E, Fuks B and Serret G 2013 *Comput. Phys. Commun.* **184** 222–256 (*Preprint* 1206.1599)
[30] Conte E, Dumont B, Fuks B and Wymant C 2014 *Eur. Phys. J.* **C74** 3103 (*Preprint* 1405.3982)
[31] Conte E and Fuks B 2018 *Int. J. Mod. Phys.* **A33** 1830027 (*Preprint* 1808.00480)
[32] Khachatryan V *et al.* (CMS) 2015 *JHEP* **06** 121 (*Preprint* 1504.03198)
[33] Backovic M, Kramer M, Maltoni F, Martini A, Mawatari K and Pellen M 2015 *Eur. Phys. J.* **C75** 482 (*Preprint* 1508.05327)
[34] Khachatryan V *et al.* (CMS) 2015 *Eur. Phys. J.* **C75** 235 (*Preprint* 1408.3583)
[35] Mattelaer O and Vryonidou E 2015 *Eur. Phys. J.* **C75** 436 (*Preprint* 1508.00564)
[36] Khachatryan V *et al.* (CMS) 2016 *Phys. Rev. Lett.* **117** 031802 (*Preprint* 1604.08907)
[37] Khachatryan V *et al.* (CMS) 2015 *Phys. Lett.* **B750** 494–519 (*Preprint* 1506.02301)
[38] Andersen J R *et al.* (LHC Higgs Cross Section Working Group) 2013 (*Preprint* 1307.1347)
[39] Aad G *et al.* (ATLAS) 2015 *JHEP* **08** 148 (*Preprint* 1505.07018)
[40] Beck L, Blekman F, Dobur D, Fuks B, Keaveney J and Mawatari K 2015 *Phys. Lett.* **B746** 48–52 (*Preprint* 1501.07580)
[41] Khachatryan V *et al.* (CMS) 2014 *JHEP* **11** 154 (*Preprint* 1409.7339)
[42] Abbiendi G *et al.* (OPAL) 2002 *Phys. Lett.* **B545** 272–284 [Erratum: Phys. Lett.B548,258(2002)] (*Preprint* hep-ex/0209026)
[43] Sirunyan A M *et al.* (CMS) 2018 *Phys. Rev.* **D97** 032009 (*Preprint* 1711.00752)
[44] The CMS Collaboration (CMS) 2017 *CMS-PAS-SUS-16-052*
[45] Aaboud M *et al.* (ATLAS) 2016 *Phys. Rev.* **D94** 032005 (*Preprint* 1604.07773)
[46] Aaboud M *et al.* (ATLAS) 2016 *Eur. Phys. J.* **C76** 392 (*Preprint* 1605.03814)